

Deep Transfer Learning for Physiological Signals

Hugh Chen
Paul G. Allen School of Computer
Science and Engineering,
University of Washington
hughchen@cs.washington.edu

Scott Lundberg
Microsoft Research
scottmlundberg@gmail.com

Gabe Erion
Paul G. Allen School of Computer
Science and Engineering,
University of Washington
erion@cs.washington.edu

Jerry H. Kim
Global Innovation Exchange,
University of Washington
jerkim@uw.edu

Su-In Lee
Paul G. Allen School of Computer
Science and Engineering,
University of Washington
suinlee@cs.washington.edu

ABSTRACT

Deep learning is increasingly common in healthcare, yet transfer learning for physiological signals (e.g., temperature, heart rate, etc.) is under-explored. Here, we present a straightforward, yet performant framework for transferring knowledge about physiological signals. Our framework is called PHASE (PHysiologicAl Signal Embeddings). It i) learns deep embeddings of physiological signals and ii) predicts adverse outcomes based on the embeddings. PHASE is the first instance of deep transfer learning in a cross-hospital, cross-department setting for physiological signals. We show that PHASE’s per-signal (one for each signal) LSTM embedding functions confer a number of benefits including improved performance, successful transference between hospitals, and lower computational cost.

1 INTRODUCTION

The performance of a predictive model is largely dependent on the availability of training data. As of 2014, more than 40% of invasive, therapeutic surgeries in the US take place in hospitals with either medium or small numbers of beds [61, 69]. These institutions may lack sufficient data or computational resources to train accurate models. Further, patient privacy considerations mean larger institutions are unlikely to publicly release their patients’ data, leaving many institutions on their own. In the face of this insufficiency, one natural way to train performant models is transfer learning, which has already shown success in medical images as well as clinical text [44, 55, 63]. Particularly with the popularization of wearable sensors used for health monitoring [46], transfer learning is underexplored for physiological signals, which account for a significant portion of the hundreds of petabytes of currently available worldwide health data [50, 56].

Drawing on parallels from computer vision (CV) and natural language processing (NLP), exemplars of representation learning, physiological signals are well suited to neural network embeddings (i.e., transformations of the original inputs into a space more suitable for making predictions). In particular, CV and NLP share two notable traits with physiological signals. The first is *consistency*. For CV, the domain has consistent features: edges, colors, and other visual attributes [54, 58]. For NLP, the domain is a particular language with semantic relationships consistent across bodies of text [13]. For sequential signals, we argue that physiological patterns

are consistent across individuals. The second attribute is *complexity*. Across these domains, each one is complex enough such that learning embeddings is non-trivial. Together, consistency and complexity suggest that distinct research scientists spend time learning embeddings that may ultimately be quite similar. In order to avoid this negative externality, NLP and CV have made great progress on standardizing and evaluating their embeddings; in health, physiological signals are a natural next step.

Furthermore, physiological signals have unique properties that make them better suited to representation learning. First, physiological signals are prevalent in health data, which is constrained by patient privacy concerns. These concerns make sharing data between hospitals difficult; however, sharing models between hospitals does not directly expose patient information. Second, a key component to successful transfer learning is a community of researchers that work on related problems. According to Faust et al. [23], there were at least 53 research publications using deep learning methods for physiological signals in the past ten years. We discuss additional examples of neural networks for physiological signals in Section 1.1.

Broadly, the goal of this manuscript is to address heterogeneous domain adaptation in a physiological signal setting. Domain adaptation is a field that aims to transfer models trained in a source domain to a target domain with a different underlying distribution (i.e., distribution divergence) [18]. *Heterogeneous* domain adaptation seeks to address the same problem, but the source and target domains may have different sets of features. This setting is of particular importance for physiological signal data, because different hospitals often measure different physiological signals.

Work discussing domain adaptation for healthcare applications exists: Choi et al. [10] investigated graph-based attention models for representation learning in healthcare, Choi et al. [11] investigated multi-layer representation learning for medical concepts. These methods do not focus on physiological signals and instead focus primarily on medical codes and concepts from temporally ordered electronic health record (EHR) visit data. Alternatively, Wiens et al. [70] investigate transfer learning in a cross-hospital setting, with the assumption of heterogeneity of features across hospitals. This approach differs to ours in that they do not utilize physiological signals and focus on linear classifiers instead of deep

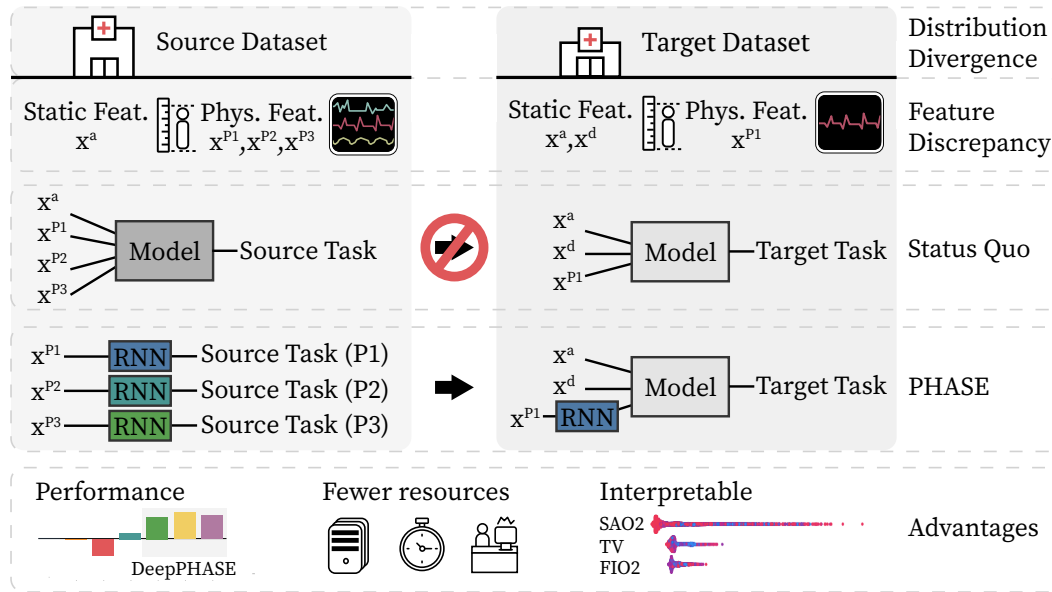


Figure 1: The PHASE framework aims to address distribution divergence between a source and target data set even in the presence of feature discrepancy. While the naive approach of transferring a single model trained on all features in the source domain will not naively work in the presence of heterogeneous features, PHASE trains an LSTM for each signal in the source domain and transfers the models to the target domain. Our approach affords a number of benefits including improved performance, lower computational cost, and preserved explainability.

networks. Another related piece of work, Gupta et al. [28] investigate transferring a single network in a clinical time series data set using recurrent neural networks. We differ in that we create several per-signal embeddings that can address heterogeneous feature sets in a cross-hospital setting.

Our approach, PHASE (PHysiological SignAl Embeddings), learns an embedding function (feature extractor) for each physiological signal. Then, utilizing these embeddings in a target data set, we train a downstream prediction model for a different, but related task (Figure 1). In particular, our contributions are the following:

- (1) We demonstrate that in comparison to the raw signals or naive transformations of the signals (exponential moving averages and variances), using LSTM feature extractors for the signals significantly improves predictive accuracy for XGB downstream models (Section 3.2.2) and for MLP downstream models (Appendix Section 7.3) used to forecast five downstream tasks in an operating room: hypoxemia (low blood oxygen), hypotension (low blood pressure), hypocapnia (low end tidal carbon dioxide), hypertension (high blood pressure), and phenylephrine administration.
- (2) We demonstrate that transferring fixed LSTM models across two distinct hospitals (a general academic medical center and a level one trauma center) yields performant downstream models. Furthermore, we show that in a heterogeneous setting, transferring from an ICU data set to both OR data sets is performant.
- (3) We demonstrate that fine tuning transferred models reduces computational cost relative to training from scratch and consistently improves performance.

- (4) We demonstrate that despite using embedding models, PHASE still allows meaningful explanation of downstream models because it uses a single LSTM for each signal.

1.1 Related work

1.1.1 Representation learning in the health domain. One particularly natural instance of representation learning in the health domain is medical image analysis, e.g., mammography analysis, kidney detection in ultrasound images, optical coherence tomography image analysis, diagnosing pneumonia using chest X-ray images, lung pattern analysis, otitis media image analysis, and more [1, 12, 34, 38, 55, 57]. Outside of image analysis, additional examples of transfer learning in the medical domain include Lv et al. [44], Wiens et al. [70], Brisimi et al. [4], Choi et al. [11], Choi et al. [10], and Che et al. [7]. Even within physiological signals, some examples of embedding learning are beginning to sprout up, including Wu et al. [72], who utilize kNNs to perform transfer learning for brain-computer interaction. Comparatively, PHASE transfers neural networks as embedding functions.

1.1.2 Neural networks for physiological signals: To our knowledge, our work is among the first to transfer deep neural networks for embedding physiological signals. One caveat is that supervised deep learning can be said to inherently learn embeddings. In physiological signals, there are several examples of particular supervised learning tasks with neural networks. Tasks ranging from detecting biological/mental phenomena from physiological signals [5, 26, 36, 60, 68, 71, 73] to machine learning tasks such as reconstruction of missing signals [62]. In the vein of embedding learning,

Martinez et al. [48] applied autoencoders to blood volume pulse and skin conductance measured from 36 people and used the encodings to predict affective state. Based on this substantive community of research scientists working on physiological signals, there is a clear opportunity to unify independent research by appropriately using partially supervised feature embedding learning.

Two pieces of work that utilize transfer learning for physiological signals include Gupta et al. [27] and Tan et al. [64]. Gupta et al. [27] transfers a single network in a clinical time series data set. Tan et al. [64] investigates transferring networks for EEG data by characterizing the data using EEG optical flow. We differ from these previous approaches by utilizing per-signal networks (one for each physiological signal) to create embeddings. Furthermore, we evaluate our method in a real world cross-hospital, cross-department setting.

1.1.3 Forecasting health outcomes. We are interested in forecasting five health outcomes. The first is hypoxemia (low blood oxygen). At one time, hypoxemia was the leading cause of anesthesia-related mortality prior to the adoption of pulse oximetry and anesthesia monitoring standards [14, 15]. Today, hypoxemia remains an important cause of anesthesia-related morbidity, precipitated by acute heart failure [17], acute renal failure [3], and harmful effects on nearly every end organ in a variety of animal models [22, 37]. The next three outcomes we consider are hypocapnia (low blood carbon dioxide), hypotension (low blood pressure), and hypertension (high blood pressure). Negative physiological effects associated with hypocapnia include reduced cerebral blood flow and reduced cardiac output [53]. Prolonged episodes of perioperative hypotension have been associated with postoperative myocardial ischemic events and other adverse postoperative outcomes [6, 39] and hypotension has been tied to increased mortality risk in traumatic brain injury patients [30]. It is generally known that hypertension is linked to premature death by heart disease, ischemia, and stroke [29, 52]. In perioperative settings, hypertension has been tied to increased risk of postoperative intracranial hemorrhage in craniotomies [2] and end organ dysfunction [66]. The final outcome we are interested in forecasting is the administration of phenylephrine. Phenylephrine is a medication frequently used to address hypotension during anesthesia administration [33]. Predicting phenylephrine would provide useful information about a patient’s hypotension and its response to phenylephrine. It also serves to further evaluate PHASE because it represents a “clinical decision” rather than just patient physiology.

Papers that discuss forecasting hypoxemia (low blood oxygen) include Coopersmith et al. [16], Lundberg et al. [43], Zhang et al. [74]. In particular, Lundberg et al. [43] most recently proposed an approach which achieved state-of-the-art performance forecasting hypoxemia. They show that an XGBoost model with exponential moving average/variance features (analogous to *ema* in Figure 2) outperforms many other baselines including practicing anesthesiologists in a simulated setting. One goal of PHASE is to replace the manual feature extraction in Lundberg et al. [43] with a deep learning approach to further improve performance. Additionally, there are papers that discuss forecasting hypotension [9, 47] and hypertension [45]; however, these papers do not consider transfer learning and focus purely on classification.

2 METHODS

2.1 Data cohort

Data Set	OR ₀	OR ₁	ICU _p
Department	OR	OR	ICU
# Procedures	29,035	28,136	1,669
Gender (F/M)	57%	38%	44%
Age (yr) Mean	51.859	48.701	63.956
Age (yr) Std.	16.748	18.419	17.708
Weight (lb) Mean	185.273	181.608	176.662
Weight (lb) Std.	54.042	54.194	55.448
Height (in) Mean	66.913	67.502	66.967
Height (in) Std.	8.268	8.607	6.181
ASA Code I	11.58%	16.57%	-
ASA Code II	41.16%	43.93%	-
ASA Code III	39.52%	31.57%	-
ASA Code IV	7.54%	7.30%	-
ASA Code V	0.19%	0.48%	-
ASA Code VI	0.01%	0.16%	-
ASA Code Emergency	7.65%	15.31%	-
# Hypoxemia Samples	3.92×10^6	4.17×10^6	5.08×10^6
Hypoxemia Base Rate	1.09%	2.19%	3.93%
# Hypocapnia Samples	1.26×10^6	1.75×10^6	-
Hypocapnia Base Rate	9.76%	8.06%	-
# Hypotension Samples	1.84×10^6	2.33×10^6	-
Hypotension Base Rate	7.44%	3.53%	-
# Hypertension Samples	2.47×10^6	2.53×10^6	-
Hypertension Base Rate	1.70%	1.66%	-
# Phenylephrine Samples	2.69×10^6	2.00×10^6	-
Phenylephrine Base Rate	7.23%	9.15%	-

Table 1: Statistics of the train validation set for different data sources.

The operating room (OR) data sets were collected via the Anesthesia Information Management System (AIMS), which includes static information as well as real-time measurements of physiological signals sampled minute by minute. OR₀ is drawn from an academic medical center and OR₁ is drawn from a trauma center. Two clear differences between the patient distributions of OR₀ and OR₁ are the gender ratio (57% females in the academic medical center versus 38% in the trauma center) and the proportion of ASA codes that are classified as emergencies (7.65% emergencies versus 15.31%). ICU_p is a sub-sampled version of the publicly available MIMIC data set from PhysioNet, which contains data obtained from an intensive care unit (ICU) in Boston, Massachusetts [31]. Although the ICU_p data contains several physiological signals sampled at a high frequency, we solely use a minute by minute SaO₂ signal for our experiments because other physiological signals had a substantial amount of missingness. Furthermore, the ICU_p data contained neonatal data that we filtered out. For all three data sets, any remaining missing values in the signal features are imputed by the mean and each feature is standardized to have unit mean and variance for training neural networks. Additional details about the distributions of patients in all three data sets are in Table 1 and a list of the prevalent diagnoses are in Appendix Section 7.1.

In the OR data sets, we utilize fifteen physiological signals:

- *SAO2* - Blood oxygen saturation
- *ETCO2* - End-tidal carbon dioxide
- *NIBP[S|M|D]* - Non-invasive blood pressure (systolic, mean, diastolic)
- *FIO2* - Fraction of inspired oxygen
- *ETSEV/ETSEVO* - End-tidal sevoflurane
- *ECGRATE* - Heart rate from ECG
- *PEAK* - Peak ventilator pressure
- *PEEP* - Positive end-expiratory pressure
- *PIP* - Peak inspiratory pressure
- *RESPRATE* - Respiration rate
- *TEMP1* - Body temperature

In addition, we utilize six static features: *Height*, *Weight*, *ASA Code*, *ASA Code Emergency*, *Gender*, and *Age*.

2.2 Downstream Prediction Tasks

In order to validate our embeddings, we focus on health forecasting tasks; forecasting tasks facilitate preventative healthcare by enabling healthcare providers to mitigate risk preemptively [59]. In particular, we consider the following five tasks:

- *Hypoxemia*: is blood oxygen less than 93 in the next five minutes of surgery ($\min(SAO2_{t+1:t+6}) < 93$)?
- *Hypocapnia*: is end tidal carbon dioxide less than 35 in the next five minutes of surgery ($\min(ETCO2_{t+1:t+6}) < 35$)?
- *Hypotension*: is mean blood pressure less than 60 in the next five minutes of surgery ($\min(NIBPM_{t+1:t+6}) < 60$)?
- *Hypertension*: is mean blood pressure higher than 110 in the next five minutes of surgery ($\min(NIBPM_{t+1:t+6}) > 110$)?
- *Phenylephrine*: is phenylephrine administered in the next five minutes of surgery ($\text{any}(PHENYL_{t+1:t+6})$)?

For more detailed information regarding our labelling schemes, refer to Section 7.2.

2.3 PHASE

In this section, we describe PHASE. Informally, PHASE first trains one neural network (upstream embedding model) for each physiological signal in a source data set (Figure 1). Then, the network without its final output layer serves as the embedding function, because neural networks implicitly learn representations of their inputs in intermediate layers. This gives a mapping from the original signal space to a latent space that is easier to make predictions in. After this, we evaluate the embedding models by training a downstream prediction model on target data pre-processed by the upstream embedding models. This confers advantages including better performance and fewer computational resources.

More formally, we train our upstream embedding models as follows: one neural network $U^i : \mathbb{R}^{n_{time}} \rightarrow \mathbb{R}^1$ for each signal $S^i \in \mathbb{R}^{n_{time}}$, $i = 1 \dots, n_{sig}$ where we draw batches from a source data set D_s (n_{time} is the number of minutes and n_{sig} is the number of signals). Because these embedding models are neural networks, we can define $H(U^i) : \mathbb{R}^{n_{time}} \rightarrow \mathbb{R}^{n_{hid}}$, to return a vector of the activations prior to the final dense layer of the network U^i (n_h is the number of hidden nodes of the penultimate layer). Then, the embedding of a given signal S^i can be written as $H(U^i) \in \mathbb{R}^{n_{hid}}$. Then, we train our downstream prediction model $D : \mathbb{R}^{n_{hid} \times n_{sig} + n_{static}} \rightarrow \mathbb{R}^1$ on data from a target domain D_t .

Here, the inputs are in $\mathbb{R}^{n_{hid} \times n_{sig} + n_{static}}$ because we use the upstream embedding models to extract features from all signal data ($n_{hid} \times n_{sig}$) from D_t and concatenate with the static features (n_{static}).

2.3.1 Upstream embedding model (LSTM). Our embedding models U^i are LSTMs trained with the last sixty minutes of each signal S^i as an input. We choose LSTMs because our physiological signal data is time series in nature. Although training the LSTMs is relatively straightforward, an important design decision is the choice of source task for training the LSTM. One trivial option is a source task that matches the downstream task exactly. In other words, if you know you want to forecast hypoxemia, simply train all embedding models to forecast hypoxemia (*hypo* in Figure 1a). Analogously, for hypocapnia, train all embedding models to forecast hypocapnia and for hypotension, train all embedding models to forecast hypotension. One clear downside of this approach is that the resultant embeddings will be specific to the chosen source task and likely be less helpful for forecasting other outcomes (task adaptation). Furthermore, in Section 3.2.2 we find that using such a specific source task is unnecessary and in Section 3.2.3 we find that it does not transfer well.

In order to choose a loss function for the LSTM, we train the LSTMs with different source tasks/outputs (i.e., the task used to train the embeddings) in order of distance to the target task (outlined in Figure 2a).

- The first output we try to predict is exactly the same as the the downstream task, all fifteen LSTMs U^i are trained to forecast either hypoxemia, hypocapnia, or hypotension using S^i as the input (*hypo*; e.g., $y = \min(SAO2_{t+1:t+6}) < 93$, $y = \min(ETCO2_{t+1:t+6}) < 35$, or $y = \min(NIBPM_{t+1:t+6}) < 60$).
- For the next three source tasks, we train U^i with an output from the signal S^i that is used as input. In particular, we start by specifying our interest in forecasting low signals (*min*; e.g., $y = \min(S^i_{t+1:t+6})$).
- Then we omit the minimum function and focusing on forecasting (*next*; e.g., $y = S^i_{t+1:t+6}$).
- Then, as a baseline we omit our emphasis on forecasting (*auto*; e.g., $y = S^i_{t-59:t}$).
- Finally, we omit the training process altogether (*rand*).

The less similar the source task is to the target task, the more likely the features extracted by the LSTM will generalize to other tasks. Conversely, if the source task is more similar to the target task, we would expect a downstream model trained on the extracted features to be more performant. Once we have trained these models in a given source domain D_s , we obtain embeddings of the physiological signals by passing them through to the final hidden layer.

The *next*, *min*, and *auto* embeddings are unsupervised in the sense that training them requires only one signal (at different time steps). Yet, they are supervised because we find that a fully unsupervised approach (*auto*) is not performant for forecasting adverse outcomes (Section 3.2.2). We recommend the utilization of the *next* task as the source task on the basis of prediction performance and robustness to downstream tasks (Section 3).

The aforementioned tasks use a source domain that is the same as the target domain ($D_s = D_t$). We have two additional variants:

- The first is denoted by an apostrophe ($'$). This signifies that if the target data set (where the XGBoost model is trained) is OR_0 , the source data set (where the LSTMs are trained) is OR_1 (and vice versa).
- The second is denoted by a superscript P (P). This signifies that the LSTM for SAO_2 is from ICU_P and the remaining fourteen LSTMs are from the target operating room data set. This constitutes a heterogenous setting where we determine whether the SAO_2 feature extractor from an ICU can be used in conjunction with ones from an OR.

One reason we use per-signal networks (trained on a single signal) is heterogeneity in features. By using per-signal networks, the source data set and target data set can have different sets of features. The traditional transfer learning approach of transferring a single end to end model in heterogenous settings often leads to a drop in performance due to missing features. For PHASE, one can simply find LSTMs for all the signals in their data set and flexibly use them as feature extractors for a downstream model. Another reason for per-signal networks is that data in a single hospital is often collected at different points in time, or new measurement devices may be introduced to data collection systems. For traditional pipelines, it may be necessary to re-train entire machine learning pipelines when new features are introduced. With per-signal networks, pre-existing embedding learners would not necessarily need to be re-trained. A final reason for using per-signal networks is that it makes explanation of downstream models easier (Section 3.3).

3.2.2 Downstream prediction model (XGB). PHASE can use any prediction model for the target task. In this paper, we focus on gradient boosting machine trees because prior work found that they outperform several other models for the operating room data we use [43]. Gradient boosting machines were introduced by Friedman [24]. This technique creates an ensemble of weak prediction models in order to perform classification/regression tasks in an iterative fashion. In particular, we utilize XGBoost, a popular implementation of gradient boosting machines that uses additive regression trees [8]. In Kaggle, a platform for predictive modeling competitions, seventeen out of twenty nine challenge winning solutions used XGBoost in 2015 [8]. For PHASE, we find that utilizing embeddings of time series signals provides stronger features for the ultimate prediction with XGB (Section 3.2.1).

3 RESULTS

3.1 Experimental Setup

3.1.1 LSTM (upstream embedding) architecture and training. We utilize LSTMs with forget gates, introduced by Gers et al. [25], implemented in the Keras library with a Tensorflow back-end. We train our networks with either regression (*auto* and *min* embeddings) or classification (*hypo*) objectives. For regression, we optimize using Adam with an MSE loss function. For classification we optimize using RMSProp with a binary cross-entropy loss function (additionally, we upsample to maintain balanced batches during training). Our model architectures consist of two hidden layers, each with 200 LSTM cells with dense connections between all layers. We found

that important steps in training LSTM networks for our data are to impute missing values by the training mean, standardize data, and to randomize sample ordering prior to training. To prevent overfitting, we utilized dropouts between layers as well as recurrent dropouts for the LSTM nodes. We utilized a learning rate of 0.001. Hyperparameter optimization was done by manual coordinate descent. The LSTM models were each run for 200 epochs and the final model was selected according to validation loss. In order to train these models, we utilize three GPUs (GeForce GTX 1080 Ti graphics cards).

3.1.2 GBM (downstream prediction) architecture and training. We train GBM trees in Python using XGBoost, an open source library for gradient boosting trees. XGBoost works well in practice in part due to its ease of use and flexibility. Imputing and standardizing are unnecessary because GBM trees are based on splits in the training data, so that scale does not matter and missing data is informative as is. We train the GBM trees with embedding features from 15 physiological signals, resulting in a total of 3000 features for DeepPHASE methods. In addition, we concatenate static features to the signal features to train and evaluate the models. We found that a learning rate of 0.02 for hypoxemia (0.1 for hypotension and hypocapnia), a max tree depth of 6, subsampling rate of 0.5, and a logistic objective gave us good performance. We fix hyperparameter settings across experiments so that we can focus on comparing different representations our signal data. All XGB models were run until their validation accuracy was non-improving for five rounds of adding estimators (trees). In order to train these models, we utilize 72 CPUs (Intel(R) Xeon(R) CPU E5-2699 v3 @ 2.30GHz)

3.2 Evaluating the performance of PHASE

In the following section we describe the application of PHASE to the problem of forecasting adverse outcomes. Our metric of evaluation is area under a precision recall curve, otherwise known as average precision (AP), which is often preferable for binary predictions with low base rates. As a brief overview of the following sections:

- (1) First, we establish baselines by comparing downstream models (LSTM to XGB) and a method comparable to practicing anesthesiologists (Lundberg et al. [43]) (Section 3.2.1). Building upon these baselines, we evaluate PHASE, which uses a combination of LSTM feature extractors and a downstream XGB model, for three “hypo” tasks (*hypoxemia*, *hypocapnia*, and *hypotension*). To show that PHASE embedding functions work for a variety of downstream models, we also benchmark using a downstream MLP model in Appendix Section 7.3.
- (2) In order to find the best task to train our LSTMs with, we explore a setting where the LSTMs are learned in the same target domain as the downstream XGB model (Section 3.2.2) and then in a setting where the LSTMs are learned in a different source domain to the target domain the XGB model is trained in (Section 3.2.3). For these sections, we focus on forecasting *hypoxemia*, *hypocapnia*, and *hypotension*.
- (3) To further evaluate PHASE, we utilize two non-“hypo” downstream tasks, namely *hypertension* and *phenylephrine* (Section 3.2.4).

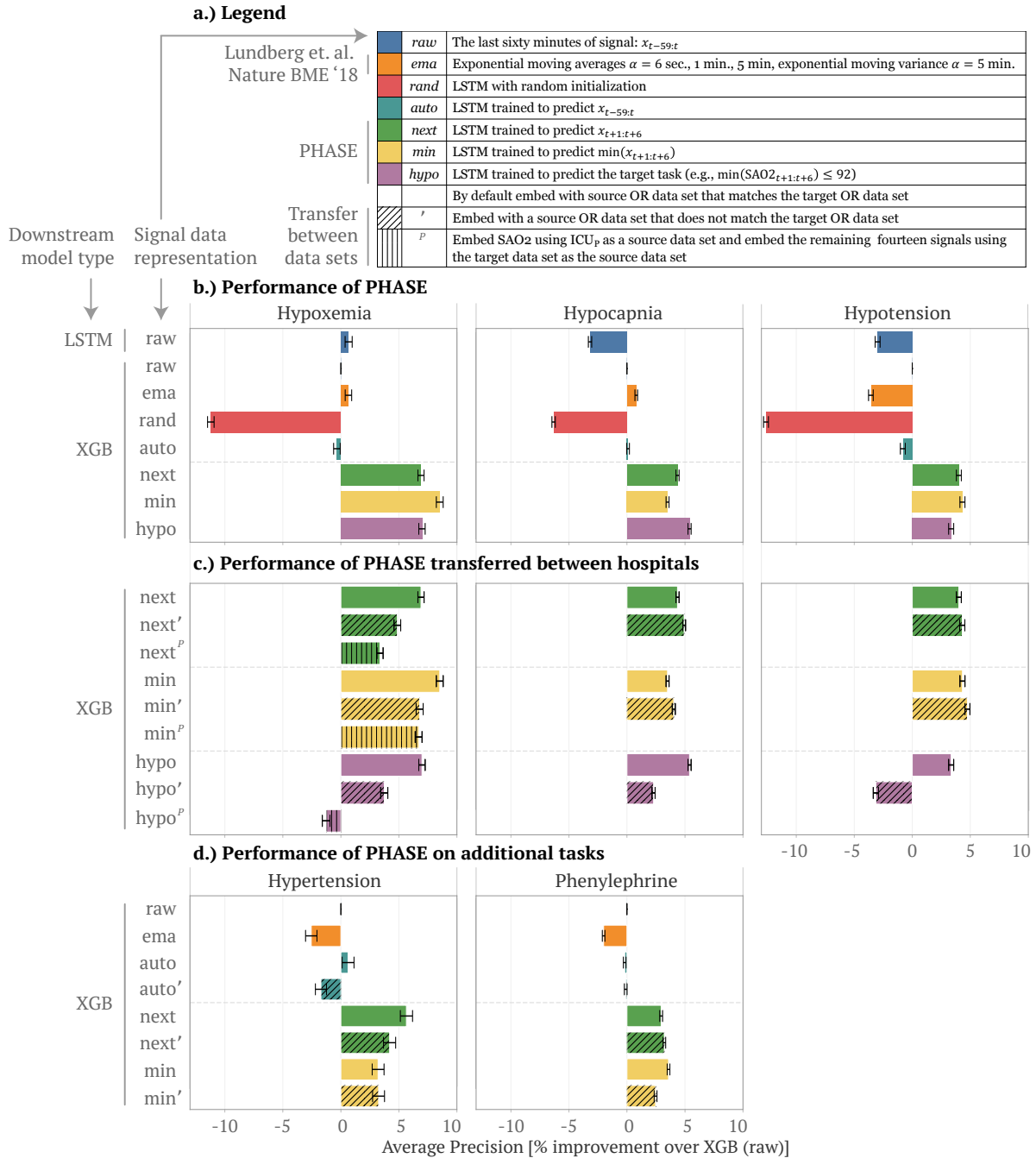


Figure 2: Average precision (% improvement over XGB model trained with *raw* signal data, 99% confidence intervals from bootstrap resampling of the test set) of XGB run with different representations of the physiological signals concatenated to static features. We use OR₀ and OR₁ as target data sets in turn, then aggregate across both by averaging the resultant means and standard errors. In (a), we describe the ways in which we represent the physiological signals. In (b), we report the performance of stacked models and see that models trained with PHASE embeddings consistently improve performance. In (c), we report the performance of transferred models as compared to non-transferred baselines. We see that transferred models are generally successful, possibly with the exception of transferred *hypo* models. Finally, in (d), we apply the embeddings to non-hypo tasks and see that *next* embeddings transfer well for forecasting hypertension and phenylephrine.

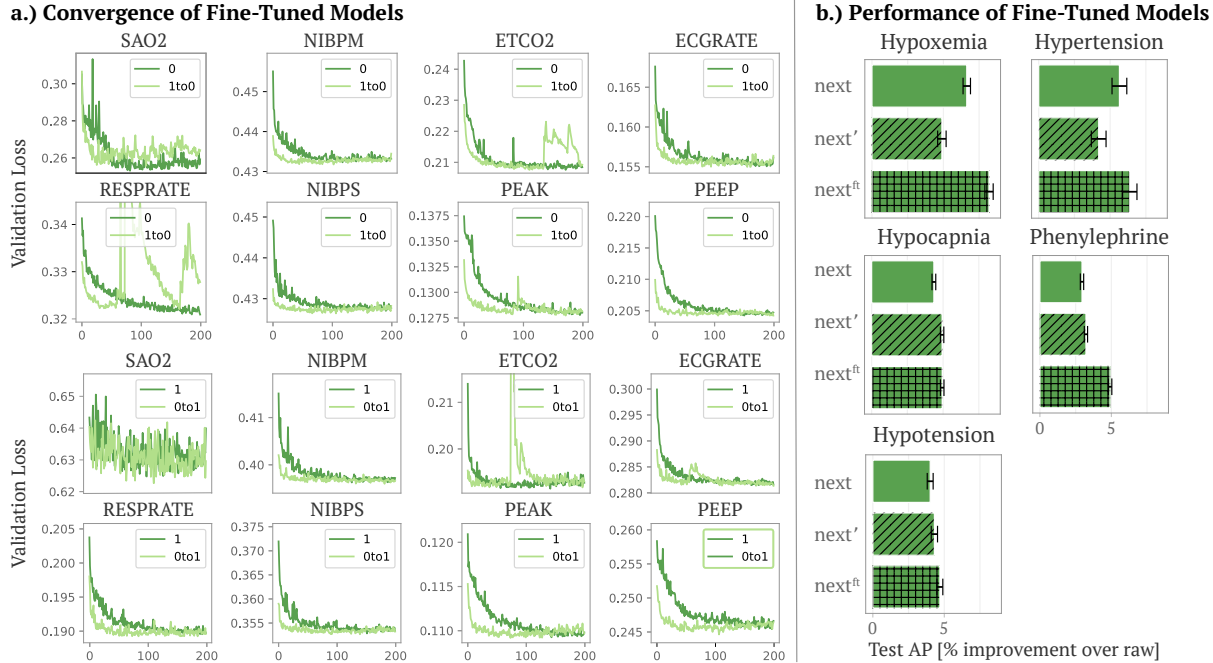


Figure 3: Convergence/performance of fine tuned models. In (a), we show the convergence of fine-tuned models. The top eight plots are trained on OR_0 and the bottom eight are trained on OR_1 (we plot eight features out of the total fifteen). The light green lines correspond to fine tuned models. In (b), we show the performance of XGB trained on embeddings from non-transferred models (*next*), transferred models (*next'*), and fine-tuned models (*next^{ft}*) on a separate test set by selecting the best embedding models according to their validation loss (in a).

(4) Finally, we examine how fine tuned versions of the *next* LSTMs (trained in one OR data set and fine tuned in the other) converge and perform compared to models trained from scratch (Section 3.2.5).

3.2.1 Establishing our baselines. In Figure 2b, we make a number of comparisons. Our first goal is to compare two downstream models: XGBoost and an LSTM (both trained on *raw* signal data). In order to obtain the best LSTM baseline, we hyperparameter tuned over the number of LSTM layers (1,2,3), number of nodes (100,200,300), optimizers (RMSProp, SGD, Adam), learning rates (0.01,0.001,0.0001), and dropout rates (0,0.5) for forecasting *hypoxemia* on OR_0 and used the best model for subsequent analyses. Comparing these models we see that an end to end LSTM model marginally helps for *hypoxemia* forecasting and hurt for *hypocapnia* and *hypotension*. This result is surprising given that one might expect LSTMs to be more suitable to time series data. In comparison, we aim to evaluate PHASE which utilizes both model types to further improve performance (Section 3.2.2).

Next, we examine a natural baseline: *ema* - a simple yet surprisingly effective representation. In fact, Lundberg et al. [43] previously showed that XGBoost with *ema* features outperformed practicing anesthesiologists for forecasting hypoxemia in a simulated setting. However, while the *ema* representation encodes much of the information from the original data, it does not significantly improve performance compared to *raw* (*hypoxemia*, *hypotension*) and at times even hurts performance (*hypotension*).

3.2.2 PHASE improves downstream model performance. In this section we evaluate PHASE, which uses LSTMs to extract features for each signal, that are fed into XGB downstream models. These features are concatenated to static patient information and used to train a downstream XGBoost model. In this section, the LSTMs are trained in the target dataset ($D_s = D_t$) (*next*, *min*, and *hypo* in Figure 2b). We compare to four baselines: *raw*, *ema*, *rand*, and *auto*. The first two baselines have been discussed in Section 3.2.1. The *rand* representation uses an LSTM with random weights. The *auto* representation uses an LSTM trained to predict the last 60 minutes of a signal (the same as the input). As a final note, all the downstream XGBoost models are trained with identical hyperparameters in order to fairly compare different representations of the input data.

First, *rand* transforms the data in a manner that makes it harder to perform the eventual prediction, serving as a lower bound for the performance of LSTM embeddings. Second, similarly to *ema*, *auto* does not appear to consistently improve or impair performance relative to *raw*. Third, it appears that *next*, *raw*, and *hypo* consistently yield better performing models for all three target tasks. Contrasting this result to *auto* appears to suggest that for our target tasks (forecasting binary “hypo” outcomes), incorporating the future in the source task is crucial (as in *next*), although taking the minimum (*min*) and thresholding (*hypo*) does not further improve performance. Finally, PHASE embeddings improve over *ema*, a method on par with practicing anesthesiologists (Lundberg et al. [43]).

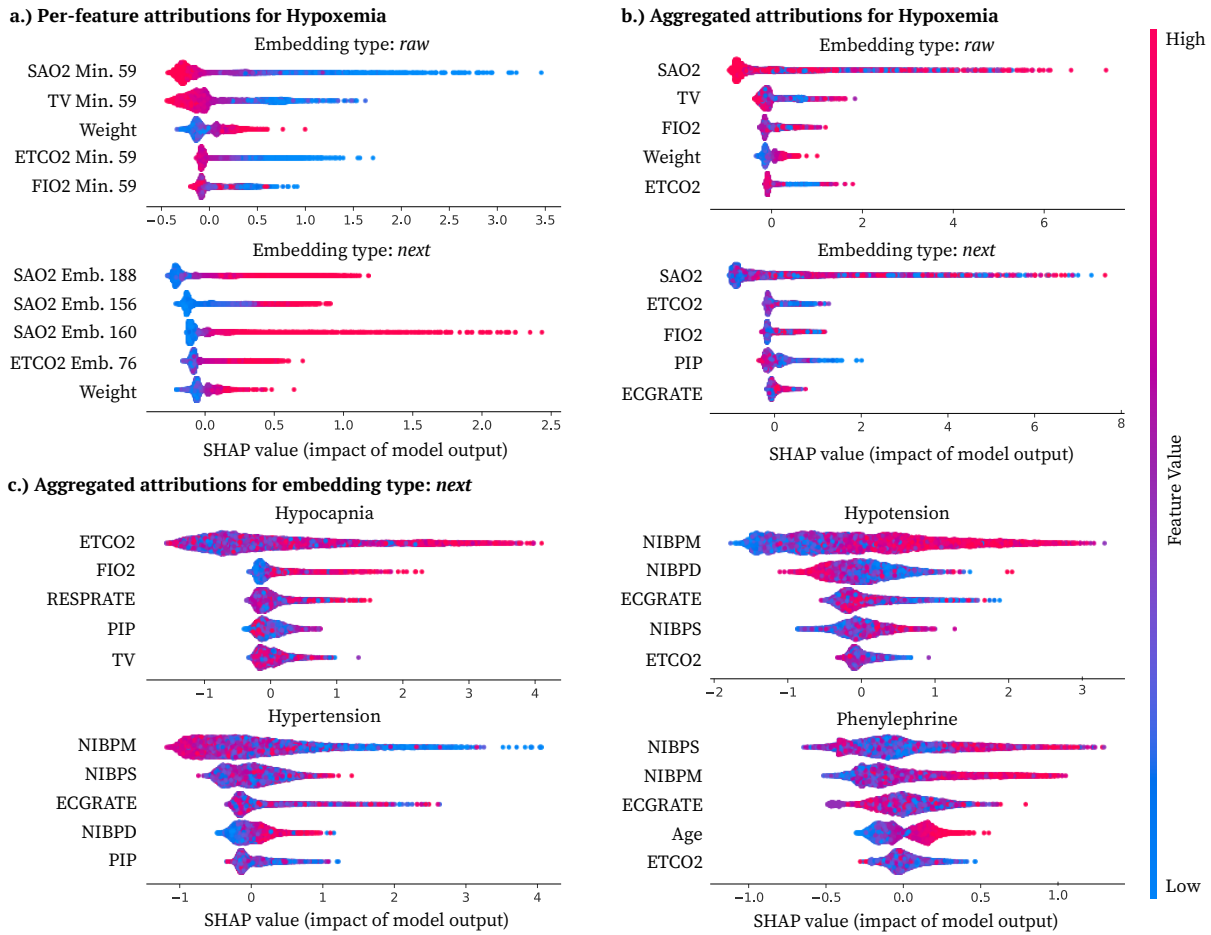


Figure 4: Local feature attributions for top five most important features from models trained in target data set OR_0 . In (a), we show attributions for *raw* and *next* models trained to forecast hypoxemia. In (b), we aggregate the attributions by signal for hypoxemia. In (c), we aggregate the attributions for the remaining four downstream tasks and plot them. For the top twenty important feature attributions, see Appendix Section 7.4

3.2.3 *PHASE transfers across hospitals successfully.* In Figure 2c, we show that the PHASE LSTM feature extractors transfer successfully across hospitals and departments. We see one trend consistent across all three target tasks. As one might expect, training the LSTMs on a source data set that is different than the target data set ($D_s \neq D_t$; denoted as $'$ and P) has lower downstream performance compared to LSTMs trained in the target data set ($D_s = D_t$; denoted as *next*, *min*, *hypo*).

Despite this, across the three target tasks, *next'* and *min'* significantly outperform *raw*, particularly in comparison to *hypo'*. These results suggest that the choice of source task is extremely important and having a source task that is identical to the target task (*hypo'*) is not the best for generalization. Finally, transference from ICU_P (P) is equally successful for forecasting hypoxemia in comparison to transference between OR data sets ($'$), suggesting successful transference from an intensive care unit data set to both

operating room data sets. This is particularly exciting for two reasons: 1.) because intensive care units likely serve very different populations of patients compared to operating rooms and 2.) we used an LSTM feature extractor for *SAO2* from ICU_P in conjunction with ones from the operating room data sets. For forecasting “hypo” outcomes, it appears that the best LSTM source task is either *next* or *min*. Of these two, *next* is preferable because it is likely to adapt to more downstream prediction tasks.

In summary, although transferring fixed models is consistently more performant than *raw* embeddings, it is not more performant than training the LSTMs in the target domain to begin with. However, one important advantage of transferring fixed models is that the end user the target domain can use these fixed models to improve their predictions at *no additional training cost*. End users that may lack either computational resources or deep learning expertise to train their own models from scratch can instead use an off the shelf, fixed embedding model. Given that machine learning is often

not the primary concern of hospitals, fixed models could offer a straightforward way to improve the performance of many models trained on physiological signal data.

3.2.4 Applying PHASE to additional tasks. One potential criticism of the results highlighted in Figure 2b and 2c is that they exclusively pertain to forecasting low signals (“hypo” outcomes). In Figure 2d, we evaluate PHASE on two tasks that are not “hypo” tasks. For *hypertension* (high blood pressure) we empirically demonstrate that as we would expect, *next* representations are better than *min* representations. For *phenylephrine*, we see improved performance from both the *next* and *min* models. This makes sense because phenylephrine is typically administered in response to low blood pressure. Finally, we can see that, as before, transferring fixed *next* and *min* embeddings significantly improves over *raw*, *ema*, and *auto*.

3.2.5 Fine-tuning embedding models. In this section, we describe how to improve performance of transferred models (Section 3.2.3) by fine tuning them in the target domain. Because *next* performed and generalized well in previous sections, we focus on this source task for the following experiment. In Figure 3, we aim to evaluate the convergence and performance of fine tuning the LSTM embedding models. Firstly, in Figure 3a we show the convergence of fine tuned models. In the top eight plots, we fix OR_0 to be the source data set. In green we show the convergence of a randomly initialized LSTM trained for each signal. In light green we show the convergence of an LSTM initialized using weights from the best model in OR_1 . In the bottom eight plots we show the analogous plots when OR_1 is the source data set. From these plots we can see that fine tuning LSTMs rather than training them from scratch consistently leads to much faster convergence; this suggests that end users that are capable of fine tuning LSTMs should always do so. In Figure 3b, we see that LSTMs obtained from this fine tuning approach (*next*^{ft}) consistently improve downstream model (XGB) performance in comparison to LSTMs trained in a single source data set (*next*, *next'*). Overall, fine tuning the LSTM feature extractors improves performance at lower cost to end users in the target domain.

3.3 Explanation of downstream models

In the following section we interpret the downstream models we used to evaluate our embeddings. The goal of the section is twofold: 1.) to validate that the downstream models are sensible and 2.) to demonstrate that downstream models trained using PHASE embeddings are explainable. Being able to interpret downstream models is important for ensuring models are fair/unbiased, trustable, valuable to scientific understanding, and more [20]. This is especially true when the results are used to make critical decisions involving human health.

3.3.1 Interpretation using SHAP values. In order to obtain explanations, we utilize Interventional Tree Explainer which provides exact SHAP values (feature attributions with game-theoretic properties) for complex tree-based models [41, 42]. SHAP values or feature attributions indicate how much each feature contributed to each prediction. We use SHAP values to explain which features were important for each sample’s prediction in our downstream XGB models.

In Figure 4, we plot summary plots for the top five most important features for both the *raw* and *next* XGBoost models. In these summary plots, each point represents a feature’s attribution for a given sample. The coloring denotes the value of the feature. In the embedding case, the feature value is arbitrarily chosen by the embedding model and in the aggregated attributions (c), the colors are the sum of all values from aggregated features. For both cases, the coloring of the signal features is generally not very informative.

3.3.2 Aggregating feature attributions by signal (Hypoxemia). In Figure 4a we plot attributions for XGB models trained with *raw* and *next* data. For *raw*, the attributions are in the original signal space, where each number corresponds to the minute when the value was recorded (relative to the current time step). For *next*, the attributions are in the embedding space, where each attribution corresponds to an LSTM hidden node.

In this plot we can see a few trends. The first is that in the *raw* model, most of the important features are the 59th minute from a given signal, which corresponds to the last minute of data before the prediction occurred. This makes sense because signals have temporal locality: in order to forecast the future five minutes, the most recent time points are the most helpful. Comparing across both models, we can see that *SAO2* is naturally the most important feature for both models (since we are forecasting low blood oxygen). Note that in contrast to the *raw* model, we can see that for the important *SAO2* embeddings, higher values correspond to positive predictions. Note that because these features are pre-processed, the embedding features’ values are not as naturally interpretable as minutes from *SAO2*. Next, we can see a consistent trend across both models in the static *Weight* feature: low weights are protective and high weights contribute to higher hypoxemia risk predictions. Another interesting point is that in the *next* model, three *SAO2* features are the most important as opposed to one in *raw*. This suggests that the LSTM trained to forecast the next five minutes of *SAO2* learned multiple representations of *SAO2* that serve to forecast hypoxemia risk even though we do not specifically train it to do so. These representations give the downstream model more discriminative power.

Although having the per-feature attributions are useful, in most end-user scenarios, understanding which signal contributes most to the prediction is of primary importance. Because PHASE utilizes single-signal LSTM embedding functions, we are able to obtain per-signal feature attributions despite using representation learning. In Figure 4b, we sum the attributions for each signal S^i from all features that correspond to S^i . We can see a good deal of overlap between the top features from the *raw* and *next* models. Finally, the union of the important variables from both models are all variables logically connected to blood oxygen. *SAO2*, *ETCO2*, and *FIO2* are all variables associated with the respiratory system. *TV* and *PIP* are both variables tied to mechanical ventilation and are naturally linked to blood oxygen [21, 35]. Finally, the negative correlation between BMI and lung capacity [32], the increased difficulty of ventilating heavier patients [19], and the association of obesity with many downstream effects including cardiovascular function [67] and ischemic heart disease [65] could justify the importance of *Weight* we see in Figures 4a and 4b could be that .

3.3.3 Top features for downstream tasks. In Figure 4c, we plot the aggregated attributions for *next* models trained to predict the remaining four outcomes. Once again, we can verify that the top features are appropriate. Firstly, for *hypocapnia* it is natural that *ETCO2* is the most important feature. Furthermore, it makes sense to utilize *FIO2*, *RESPRATE*, *PIP*, and *TV* to forecast hypocapnia because these variables are all related to either ventilation or respiration. As one would expect, for *hypotension* and *hypertension*, the most important variables are generally the three non-invasive blood pressure measurements: *NIBPM*, *NIBPD*, *NIBPS*. Furthermore, there are a number of studies validating the importance of *ECGRATE* (heart rate measured from ECG signals) to forecasting hypotension and hypertension [49, 51]. Finally, phenylephrine administration during surgery is typically done in response to hypotension, thus validating the importance of *NIBPS*, *NIBPM*, and *ECGRATE*. Similarly, older age being more important to forecasting Phenylephrine may be tied to age being predictive of hypotension as well as the heightened vigilance anesthesiologists have for hypotension in this higher-risk population [40].

4 CONCLUSION

This paper presents PHASE, an approach to transfer learning in the domain of physiological signals. Transfer learning for physiological signals potentially has far-reaching impacts, because neural networks inherently create an embedding before the final output layer. In light of the quantity of researchers working on neural networks for physiological signals and the lack of exploration of transfer learning in this domain, PHASE offers a potential method of collaboration that can address domain and task adaptation. PHASE embeddings offer a number of benefits including improved performance, successful transference (in fixed and fine-tuned settings), lower computational cost, and preserved explainability. Potential future work includes handling multiple sampling rates for signals in addition to addressing more signals (e.g., electrocardiograms).

5 IRB STATEMENT

The electronic data for this study was retrieved from institutional electronic medical record and data warehouse systems after receiving approval from the Institutional Review Board (University of Washington Human Subjects Division, Approval #46889). Protected health information was excluded from the data set that was used for machine learning methods.

6 ACKNOWLEDGEMENTS

We would like to thank Joseph D. Janizek, Alex Okeson, and Nicasia Beebe-Wang for their feedback on the manuscript. We would also like to thank all of the members of Professor Su-In Lee's lab for their feedback on the project. In addition, this material is based upon work supported by the National Science Foundation Graduate Research Fellowship under Grant No. DGE-1762114.

REFERENCES

- [1] John Arevalo, Fabio A González, Raúl Ramos-Pollán, Jose L Oliveira, and Miguel Angel Guevara Lopez. 2016. Representation learning for mammography mass lesion classification with convolutional neural networks. *Computer methods and programs in biomedicine* 127 (2016), 248–257.
- [2] Ayman Basali, Edward J Mascha, Iain Kalfas, and Armin Schubert. 2000. Relation between perioperative hypertension and intracranial hemorrhage after craniotomy. *Anesthesiology: The Journal of the American Society of Anesthesiologists* 93, 1 (2000), 48–54.
- [3] Mayer Brezis and Seymour Rosen. 1995. Hypoxia of the renal medulla—its implications for disease. *New England Journal of Medicine* 332, 10 (1995), 647–655.
- [4] Theodora S Brisimi, Ruidi Chen, Theofanie Mela, Alex Olshevsky, Ioannis Ch Paschalidis, and Wei Shi. 2018. Federated learning of predictive models from federated Electronic Health Records. *International journal of medical informatics* 112 (2018), 59–67.
- [5] Guillaume Chanel, Julien Kronegg, Didier Grandjean, and Thierry Pun. 2006. Emotion assessment: Arousal evaluation using EEG and peripheral physiological signals. In *International workshop on multimedia content representation, classification and security*. Springer, 530–537.
- [6] Han Soo Chang, Kazuhiro Hongo, and Hiroshi Nakagawa. 2000. Adverse effects of limited hypotensive anesthesia on the outcome of patients with subarachnoid hemorrhage. *Journal of neurosurgery* 92, 6 (2000), 971–975.
- [7] Zhengping Che, Sanjay Purushotham, Robinder Khemani, and Yan Liu. 2016. Interpretable deep models for icu outcome prediction. In *AMIA Annual Symposium Proceedings*, Vol. 2016. American Medical Informatics Association, 371.
- [8] Tianqi Chen and Carlos Guestrin. 2016. XGBoost: A Scalable Tree Boosting System. In *Proceedings of the 22nd ACM SIGKDD International Conference on Knowledge Discovery and Data Mining (KDD '16)*. ACM, New York, NY, USA, 785–794. <https://doi.org/10.1145/2939672.2939785>
- [9] X Chen, D Xu, G Zhang, and R Mukkamala. 2009. Forecasting acute hypotensive episodes in intensive care patients based on a peripheral arterial blood pressure waveform. In *2009 36th Annual Computers in Cardiology Conference (CinC)*. IEEE, 545–548.
- [10] Edward Choi, Mohammad Taha Bahadori, Elizabeth Searles, Catherine Coffey, Michael Thompson, James Bost, Javier Tejedor-Sojo, and Jimeng Sun. 2016. Multi-layer representation learning for medical concepts. In *Proceedings of the 22nd ACM SIGKDD International Conference on Knowledge Discovery and Data Mining*. ACM, 1495–1504.
- [11] Edward Choi, Mohammad Taha Bahadori, Le Song, Walter F Stewart, and Jimeng Sun. 2017. GRAM: graph-based attention model for healthcare representation learning. In *Proceedings of the 23rd ACM SIGKDD International Conference on Knowledge Discovery and Data Mining*. ACM, 787–795.
- [12] Stergios Christodoulidis, Marios Anthimopoulos, Lukas Ebner, Andreas Christe, and Stavroula Mougialakou. 2016. Multi-source transfer learning with convolutional neural networks for lung pattern analysis. *arXiv preprint arXiv:1612.02589* (2016).
- [13] Alexis Conneau, Douwe Kiela, Holger Schwenk, Loic Barrault, and Antoine Bordes. 2017. Supervised learning of universal sentence representations from natural language inference data. *arXiv preprint arXiv:1705.02364* (2017).
- [14] Jeffrey B Cooper, Ronald S Newbower, and Richard J Kitz. 1984. An analysis of major errors and equipment failures in anesthesia management: considerations for prevention and detection. *Anesthesiology* 60, 1 (1984), 34–42.
- [15] Jeffrey B Cooper, Ronald S Newbower, Charlene D Long, and Bucknam McPeck. 1978. Preventable anesthesia mishaps: a study of human factors. *Anesthesiology* 49, 6 (1978), 399–406.
- [16] Evan Joseph Coopersmith, Barbara Minsker, and Paul Montagna. 2010. Understanding and forecasting hypoxia using machine learning algorithms. *Journal of Hydroinformatics* 13, 1 (2010), 64–80.
- [17] Cecil E Cross, P Andre Rieben, Charles I Barron, and Peter F Salisbury. 1963. Effects of arterial hypoxia on the heart and circulation: an integrative study. *American Journal of Physiology-Legacy Content* 205, 5 (1963), 963–970.
- [18] Hal Daumé III. 2009. Frustratingly easy domain adaptation. *arXiv preprint arXiv:0907.1815* (2009).
- [19] Audrey De Jong, Gerald Chanques, and Samir Jaber. 2017. Mechanical ventilation in obese ICU patients: from intubation to extubation. *Critical Care* 21, 1 (2017), 63.
- [20] Finale Doshi-Velez and Been Kim. 2017. Towards a rigorous science of interpretable machine learning. *arXiv preprint arXiv:1702.08608* (2017).
- [21] Didier Dreyfuss, Paul Soler, Guy Basset, and Georges Saumon. 1988. High inflation pressure pulmonary edema: respective effects of high airway pressure, high tidal volume, and positive end-expiratory pressure. *American Review of Respiratory Disease* 137, 5 (1988), 1159–1164.
- [22] Jesse M Ehrenfeld, Luke M Funk, Johan Van Schalkwyk, Alan F Merry, Warren S Sandberg, and Atul Gawande. 2010. The incidence of hypoxemia during surgery: evidence from two institutions. *Canadian Journal of Anesthesia/Journal canadien d'anesthésie* 57, 10 (2010), 888–897.
- [23] Oliver Faust, Yuki Hagiwara, Tan Jen Hong, Oh Shu Lih, and U Rajendra Acharya. 2018. Deep learning for healthcare applications based on physiological signals: a review. *Computer methods and programs in biomedicine* (2018).
- [24] Jerome H. Friedman. 2001. Greedy function approximation: A gradient boosting machine. *Ann. Statist.* 29, 5 (10 2001), 1189–1232. <https://doi.org/10.1214/aos/1013203451>

- [25] Felix A. Gers, Jurgen Schmidhuber, and Fred Cummins. 2000. Learning to forget: Continual prediction with LSTM. *Neural Computation* 12, 10 (2000), 2451–2471.
- [26] Ling Guo, Daniel Rivero, and Alejandro Pazos. 2010. Epileptic seizure detection using multiwavelet transform based approximate entropy and artificial neural networks. *Journal of neuroscience methods* 193, 1 (2010), 156–163.
- [27] Priyanka Gupta, Pankaj Malhotra, Jyoti Narwariya, Lovekesh Vig, and Gautam Shroff. 2019. Transfer Learning for Clinical Time Series Analysis using Deep Neural Networks. *arXiv preprint arXiv:1904.00655* (2019).
- [28] Priyanka Gupta, Pankaj Malhotra, Lovekesh Vig, and Gautam Shroff. 2018. Transfer learning for clinical time series analysis using recurrent neural networks. *arXiv preprint arXiv:1807.01705* (2018).
- [29] Theodore C Janeway. 1913. A clinical study of hypertensive cardiovascular disease. *Transactions of the Association of American Physicians* 28 (1913), 333.
- [30] Elan Jeremitsky, Laurel Omert, C Michael Dunham, Jack Protetch, and Aurelio Rodriguez. 2003. Harbingers of poor outcome the day after severe brain injury: hypothermia, hypoxia, and hypoperfusion. *Journal of Trauma and Acute Care Surgery* 54, 2 (2003), 312–319.
- [31] Alistair E.w. Johnson, Tom J. Pollard, Lu Shen, Li-Wei H. Lehman, Mengling Feng, Mohammad Ghassemi, Benjamin Moody, Peter Szolovits, Leo Anthony Celi, Roger G. Mark, and et al. 2016. MIMIC-III, a freely accessible critical care database. *Scientific Data* 3 (2016), 160035. <https://doi.org/10.1038/sdata.2016.35>
- [32] Richard L Jones and Mary-Magdalene U Nzekwu. 2006. The effects of body mass index on lung volumes. *Chest* 130, 3 (2006), 827–833.
- [33] Warwick D Ngan Kee, Kim S Khaw, Floria F Ng, and Bee B Lee. 2004. Prophylactic phenylephrine infusion for preventing hypotension during spinal anesthesia for cesarean delivery. *Anesthesia & Analgesia* 98, 3 (2004), 815–821.
- [34] Daniel S Kermany, Michael Goldbaum, Wenjia Cai, Carolina CS Valentim, Huiying Liang, Sally L Baxter, Alex McKeown, Ge Yang, Xiaokang Wu, Fangbing Yan, et al. 2018. Identifying medical diagnoses and treatable diseases by image-based deep learning. *Cell* 172, 5 (2018), 1122–1131.
- [35] Ritva Kiiski, Jukka Takala, Aarno Kari, and J Milic-Emili. 1992. Effect of tidal volume on gas exchange and oxygen transport in the adult respiratory distress syndrome. *American Review of Respiratory Disease* 146 (1992), 1131–1131.
- [36] Yasuharu Koike and Mitsuo Kawato. 1995. Estimation of dynamic joint torques and trajectory formation from surface electromyography signals using a neural network model. *Biological cybernetics* 73, 4 (1995), 291–300.
- [37] PI Korner. 1959. Circulatory adaptations in hypoxia. *Physiological reviews* 39, 4 (1959), 687–730.
- [38] Shu Liao, Yaozong Gao, Aytakin Oto, and Dinggang Shen. 2013. Representation learning: a unified deep learning framework for automatic prostate MR segmentation. In *International Conference on Medical Image Computing and Computer-Assisted Intervention*. Springer, 254–261.
- [39] Andre Lienhart, Yves Auroy, Françoise Pequignot, Dan Benhamou, Josiane Warszawski, Martine Bovet, and Eric Jouglu. 2006. Survey of anesthesia-related mortality in France. *Anesthesiology: The Journal of the American Society of Anesthesiologists* 105, 6 (2006), 1087–1097.
- [40] Laurent Lonjaret, Olivier Lairez, Vincent Minville, and Thomas Geeraerts. 2014. Optimal perioperative management of arterial blood pressure. *Integrated blood pressure control* 7 (2014), 49.
- [41] Scott M Lundberg, Gabriel Erion, Hugh Chen, Alex DeGrave, Jordan M Prutkin, Bala Nair, Ronit Katz, Jonathan Himmelfarb, Nisha Bansal, and Su-In Lee. 2019. Explainable AI for Trees: From Local Explanations to Global Understanding. *arXiv preprint arXiv:1905.04610* (2019).
- [42] Scott M Lundberg and Su-In Lee. 2017. A unified approach to interpreting model predictions. In *Advances in Neural Information Processing Systems*. 4765–4774.
- [43] Scott M Lundberg, Bala Nair, Monica S Vavilala, Mayumi Horibe, Michael J Eisses, Trevor Adams, David E Liston, Daniel King-Wai Low, Shu-Fang Newman, Jerry Kim, et al. 2018. Explainable machine-learning predictions for the prevention of hypoxaemia during surgery. *Nature biomedical engineering* 2, 10 (2018), 749.
- [44] Xinbo Lv, Yi Guan, and Benyang Deng. 2014. Transfer learning based clinical concept extraction on data from multiple sources. *Journal of Biomedical Informatics* 52 (2014), 55 – 64. <https://doi.org/10.1016/j.jbi.2014.05.006> Special Section: Methods in Clinical Research Informatics.
- [45] Yu-xia Ma and Shi-gong Wang. 2010. The application of artificial neural network in the forecasting on incidence of a disease. In *2010 3rd International Conference on Biomedical Engineering and Informatics*, Vol. 3. IEEE, 1269–1272.
- [46] Sumit Majumder, Tapas Mondal, and M Deen. 2017. Wearable sensors for remote health monitoring. *Sensors* 17, 1 (2017), 130.
- [47] E Mancini, L Corazza, DC Cannarile, ML Soverini, S Cavalcanti, S Cavani, A Fiorenzi, and A Santoro. 2008. Short term variability of oxygen saturation during hemodialysis is a warning parameter for hypotension appearance. In *2008 Computers in Cardiology*. IEEE, 881–884.
- [48] Hector P Martinez, Yoshua Bengio, and Georgios N Yannakakis. 2013. Learning deep physiological models of affect. *IEEE Computational Intelligence Magazine* 8, 2 (2013), 20–33.
- [49] Jean-François Morcet, Michel Safar, Frédérique Thomas, Louis Guize, and Athanase Benetos. 1999. Associations between heart rate and other risk factors in a large French population. *Journal of hypertension* 17, 12 (1999), 1671–1676.
- [50] Christina Orphanidou. 2019. A review of big data applications of physiological signal data. *Biophysical reviews* 11, 1 (2019), 83–87.
- [51] Paolo Palatini. 2011. Role of elevated heart rate in the development of cardiovascular disease in hypertension. *Hypertension* 58, 5 (2011), 745–750.
- [52] George Pickering. 1972. Hypertension: definitions, natural histories and consequences. *The American journal of medicine* 52, 5 (1972), 570–583.
- [53] Brian Pollard and David B Gibb. 1977. Some adverse physiological effects of hypocarbia and methods of maintaining normocarbia during controlled ventilation. *Anaesthesia and intensive care* 5, 2 (1977), 113–121.
- [54] Rajat Raina, Alexis Battle, Honglak Lee, Benjamin Packer, and Andrew Y Ng. 2007. Self-taught learning: transfer learning from unlabeled data. In *Proceedings of the 24th international conference on Machine learning*. ACM, 759–766.
- [55] Hariharan Ravishanker, Prasad Sudhakar, Rahul Venkataramani, Sheshadri Thiruvankadam, Pavan Annangi, Narayanan Babu, and Vivek Vaidya. 2016. Understanding the mechanisms of deep transfer learning for medical images. In *Deep Learning and Data Labeling for Medical Applications*. Springer, 188–196.
- [56] Joachim Roski, George W Bo-Linn, and Timothy A Andrews. 2014. Creating value in health care through big data: opportunities and policy implications. *Health affairs* 33, 7 (2014), 1115–1122.
- [57] Chuen-Kai Shie, Chung-Hisang Chuang, Chun-Nan Chou, Meng-Hsi Wu, and Edward Y Chang. 2015. Transfer representation learning for medical image analysis. In *Engineering in Medicine and Biology Society (EMBC), 2015 37th Annual International Conference of the IEEE*. IEEE, 711–714.
- [58] Hoo-Chang Shin, Holger R Roth, Mingchen Gao, Le Lu, Ziyue Xu, Isabella Noguees, Jianhua Yao, Daniel Mollura, and Ronald M Summers. 2016. Deep convolutional neural networks for computer-aided detection: CNN architectures, dataset characteristics and transfer learning. *IEEE transactions on medical imaging* 35, 5 (2016), 1285–1298.
- [59] Ireneus N Soyiri and Daniel D Reidpath. 2013. An overview of health forecasting. *Environmental health and preventive medicine* 18, 1 (2013), 1.
- [60] Vairavan Srinivasan, Chikkannan Eswaran, and Natarajan Sriraam. 2007. Approximate entropy-based epileptic EEG detection using artificial neural networks. *IEEE Transactions on information Technology in Biomedicine* 11, 3 (2007), 288–295.
- [61] Claudia A. Steiner, Zeynal Karaca, Brian J. Moore, Melina C. Imshaug, and Gary Pickens. 2017. Surgeries in Hospital-Based Ambulatory Surgery and Hospital Inpatient Settings, 2014. *HCUP Statistical Brief* (2017).
- [62] AM Sullivan, Henian Xia, JC McBride, and Xiaopeng Zhao. 2010. Reconstruction of missing physiological signals using artificial neural networks. In *Computing in Cardiology, 2010*. IEEE, 317–320.
- [63] N. Tajbakhsh, J. Y. Shin, S. R. Gurudu, R. T. Hurst, C. B. Kendall, M. B. Gotway, and J. Liang. 2016. Convolutional Neural Networks for Medical Image Analysis: Full Training or Fine Tuning? *IEEE Transactions on Medical Imaging* 35, 5 (May 2016), 1299–1312. <https://doi.org/10.1109/TMI.2016.2535302>
- [64] Chuangqi Tan, Fuchun Sun, and Wenchang Zhang. 2018. Deep transfer learning for EEG-based brain computer interface. In *2018 IEEE International Conference on Acoustics, Speech and Signal Processing (ICASSP)*. IEEE, 916–920.
- [65] Mette Thomsen and Børge G Nordestgaard. 2014. Myocardial infarction and ischemic heart disease in overweight and obesity with and without metabolic syndrome. *JAMA internal medicine* 174, 1 (2014), 15–22.
- [66] Joseph Varon and Paul E Marik. 2008. Perioperative hypertension management. *Vascular health and risk management* 4, 3 (2008), 615.
- [67] RS Vasan. 2003. Cardiac function and obesity.
- [68] Johannes Wagner, Jonghwa Kim, and Elisabeth André. 2005. From physiological signals to emotions: Implementing and comparing selected methods for feature extraction and classification. In *Multimedia and Expo, 2005. ICME 2005. IEEE International Conference on*. IEEE, 940–943.
- [69] Tian Wen. 2016. An All-Payer View of Hospital Discharge to Postacute Care, 2013. *HCUP Statistical Brief* (2016).
- [70] Jenna Wiens, John Guttag, and Eric Horvitz. 2014. A study in transfer learning: leveraging data from multiple hospitals to enhance hospital-specific predictions. *Journal of the American Medical Informatics Association* 21, 4 (2014), 699–706.
- [71] Glenn F Wilson and Christopher A Russell. 2003. Real-time assessment of mental workload using psychophysiological measures and artificial neural networks. *Human factors* 45, 4 (2003), 635–644.
- [72] Dongrui Wu, Brent J Lance, and Thomas D Parsons. 2013. Collaborative filtering for brain-computer interaction using transfer learning and active class selection. *PLoS one* 8, 2 (2013), e56624.
- [73] Te-chung Issac Yang and Haowei Hsieh. 2016. Classification of acoustic physiological signals based on deep learning neural networks with augmented features. In *Computing in Cardiology Conference (CinC), 2016*. IEEE, 569–572.
- [74] L Zhang, R Mendoza-Sassi, JCH Santos, and J Lau. 2011. Accuracy of symptoms and signs in predicting hypoxaemia among young children with acute respiratory infection: a meta-analysis. *The International Journal of Tuberculosis and Lung Disease* 15, 3 (2011), 317–325.

7 APPENDIX

7.1 Top diagnoses for our data

Top ten diagnoses (OR_0):

- Cataract NOS
- Subarachnoid Hemorrhage
- Calculus of Kidney
- Complications due to other internal orthopedic device implant and graft
- Senile Cataract NOS
- Senile Cataract Unspecified
- Necrotizing Fasciitis
- Cataract
- Carpal Tunnel Syndrome
- CMP NEC D/T ORTH DEV NEC

Top ten diagnoses (OR_1):

- Malignant Neoplasm of Breast (Female) Unspecified
- Malignant Neoplasm of Breast NOS
- Atrial Fibrillation
- Morbid Obesity
- Calculus of Kidney
- Esophageal Reflux
- Malignant Neoplasm of Prostate
- Malignant Neoplasms of Bladder Part Unspecified
- PREV C-SECT NOS-DELIVER
- End stage renal disease

Top ten diagnoses (ICU_P):

- Newborn
- Pneumonia
- Telemetry
- Sepsis
- Congestive Heart Failure
- Coronary Artery Disease
- Chest Pain
- Gastrointestinal Bleed
- Altered Mental Status
- Intracranial Hemorrhage

7.2 Labelling

For *hypoxemia*, a particular time point t is labelled to be one if the minimum of the next five minutes is hypoxemic ($\min(SAO_2^{t+1:t+6}) < 93$). All points where the current time step is currently hypoxemic are ignored ($SAO_2^t < 93$). Additionally we ignore time points where the past ten minutes were all missing or the future five minutes were all missing. *hypocapnia*, *hypotension*, and *hypertension* have slightly stricter label conditions. We label the current time point t to be one if ($\min(S^{t-10:t}) > T$) and the minimum of the next five minutes is "hypo" ($\min(S^{t+1:t+5}) \leq T$). We label the current time point t to be zero if ($\min(S^{t-10:t}) > T$) and the minimum of the next ten minutes is not "hypo" ($\min(S^{t+1:t+10}) > T$). For *Hypertension*, we use $\max(S^{t+1:t+5}) \geq T$ rather than min and an analogous filtering procedure. All other time points were not considered. For *hypocapnia*, the threshold $T = 34$ and the signal S is *ETCO2*. For *hypotension* the threshold $T = 59$ and the signal S is *NIBPM*. For *hypertension* the threshold $T = 110$ and the signal S is *NIBPM*. Additionally we ignore time points where the past

ten minutes were all missing or the future five minutes were all missing. As a result, we have different sample sizes for different prediction tasks (reported in Table 1). For *phenylephrine*, we filter out procedures where phenylephrine is not administered because we would have too many negative samples otherwise.

7.3 MLP downstream model

One potential criticism of our evaluations in previous are that we evaluate with only one downstream model type: XGBoost. There are clearly a number of benefits to using tree-based methods such as ease of training, exact SHAP value attribution methods, performance on par with LSTMs for our data sets, and more. However, in order to show that *PHASE embeddings improve performance and transference for a variety of downstream model types*, we replicate Figure 2b and 2c using MLP downstream models in Figure 5. We see that, as with downstream XGB models, the PHASE embeddings offer a substantial improvement over *raw* embeddings for downstream MLP models.

We utilize multi-layer perceptrons, implemented in the Keras library with a Tensorflow back-end. We train the MLPs with embedding features from 15 physiological signals, resulting in a total of 3000 features for DeepPHASE methods. In addition, we concatenate static features to the signal features to train and evaluate the models. The model's architecture consists of the following: a dense layer with 100 nodes (with a relu activation) followed by a dropout layer with dropout rate 0.5 followed by a dense layer with 100 nodes (with a relu activation) followed by a dropout layer with dropout rate 0.5 followed by the dense output layer with one node and sigmoid activation function. We utilize a learning rate of 0.00001, adam optimizer, and binary cross entropy loss. We found that 200 epochs was sufficient for the downstream models to converge. We fix hyperparameter settings across experiments so that we can focus on comparing different representations our signal data. In order to train these models, we utilize 72 CPUs (Intel(R) Xeon(R) CPU E5-2699 v3 @ 2.30GHz)

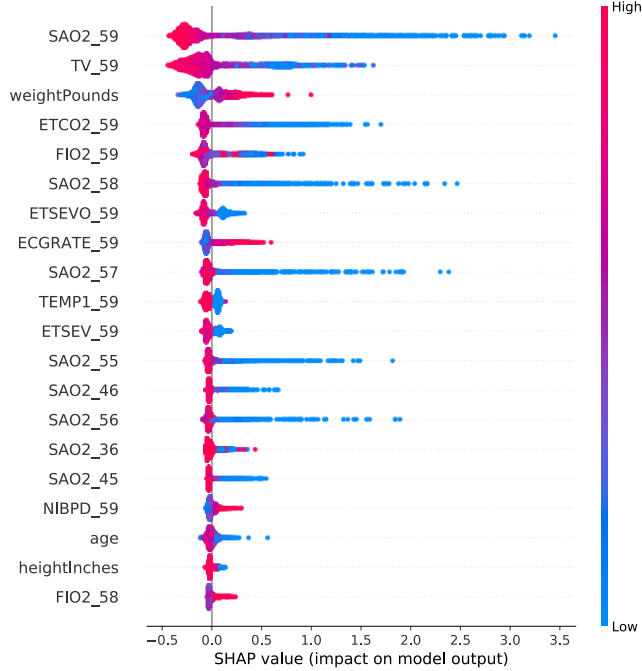
7.4 Full summary plots

In this section, we show the full summary plots (Figures 6-10) for the per-feature and aggregated attributions for *raw* and *next* models trained from XGBoost models trained in target data set OR_0 . We can see more relationships between each of the five downstream tasks and the top 20 features sorted by the mean absolute SHAP values for each feature.

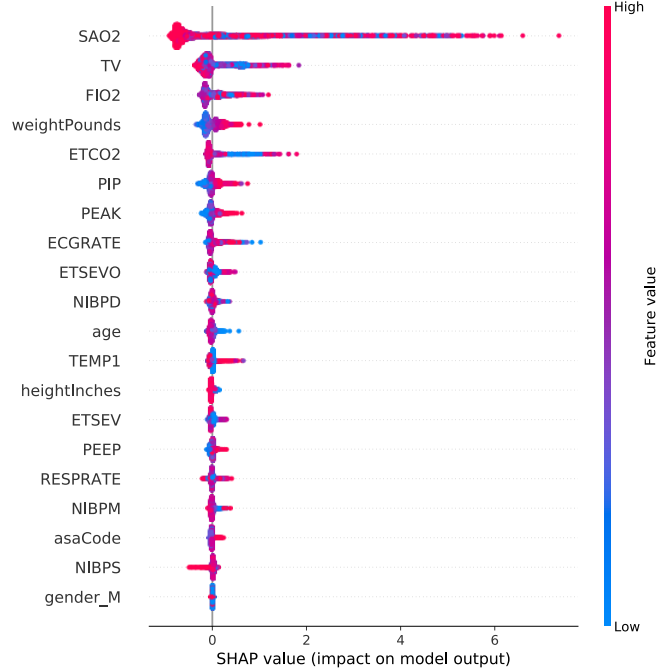


Figure 5: Performance of PHASE embeddings with MLP downstream model rather than XGB as in Figure 2.

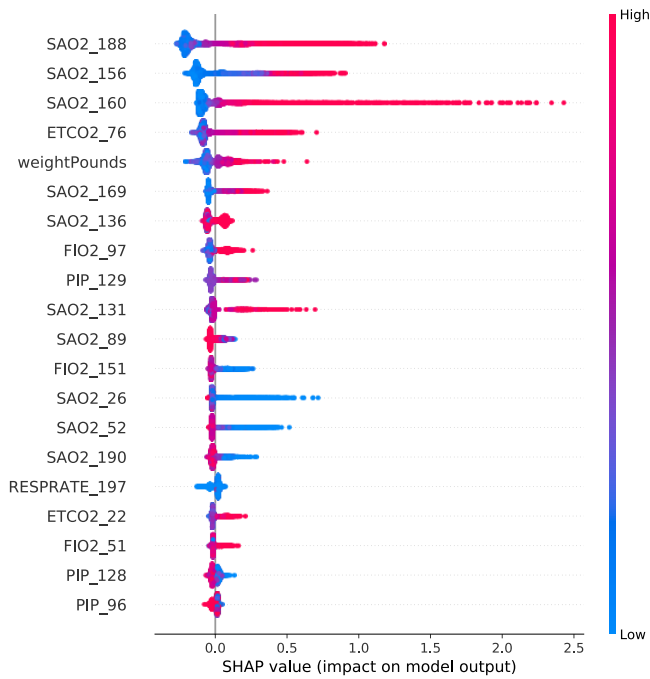
a.) Per-feature attributions for raw



b.) Aggregated attributions for raw



c.) Per-feature attributions for next



d.) Aggregated attributions for next

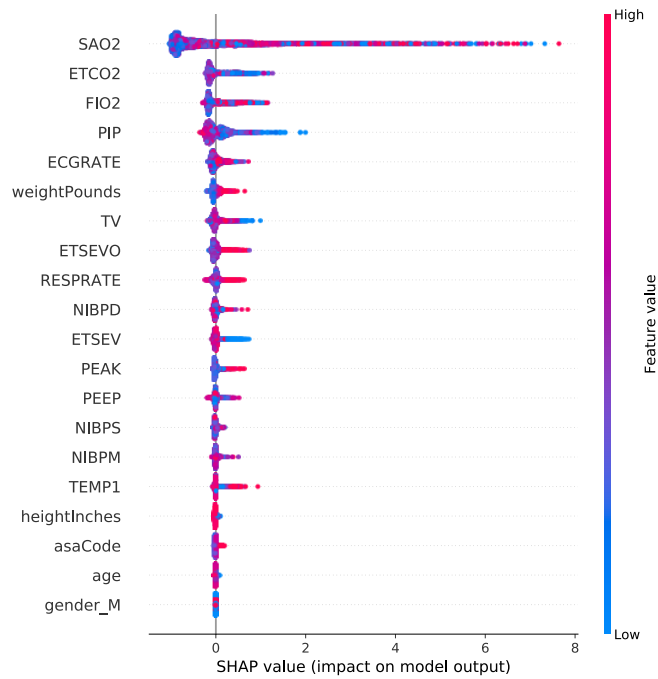
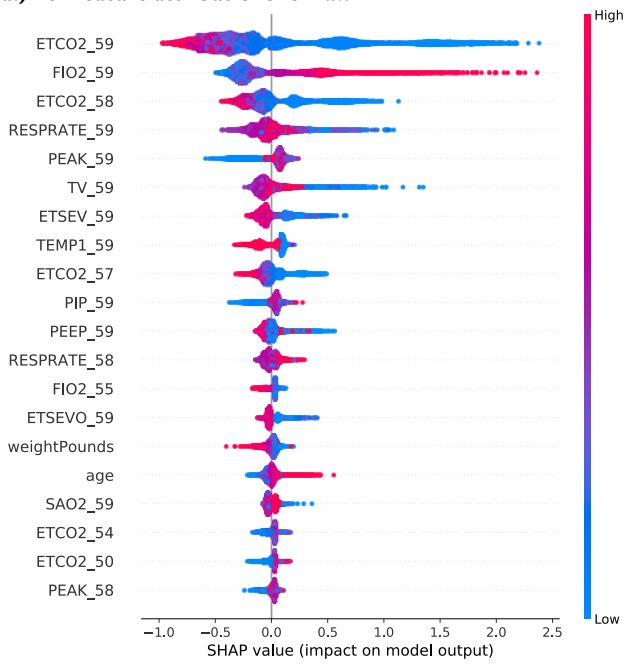
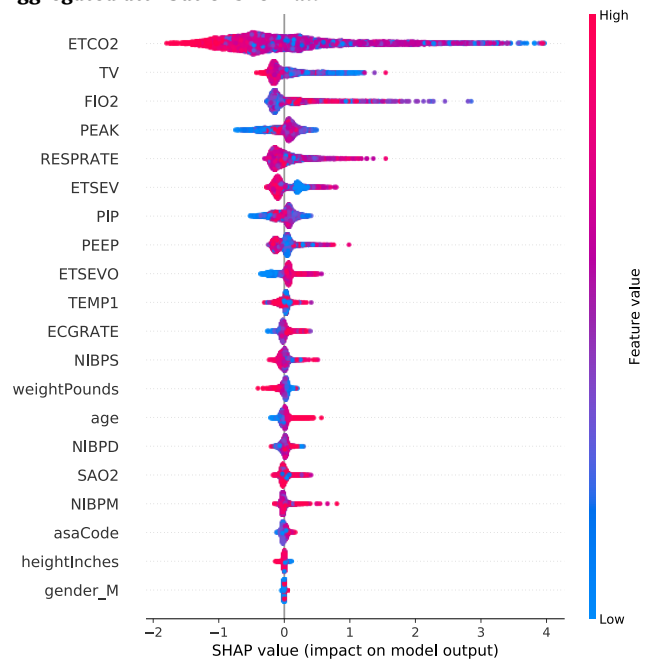


Figure 6: Attributions for hypoxemia.

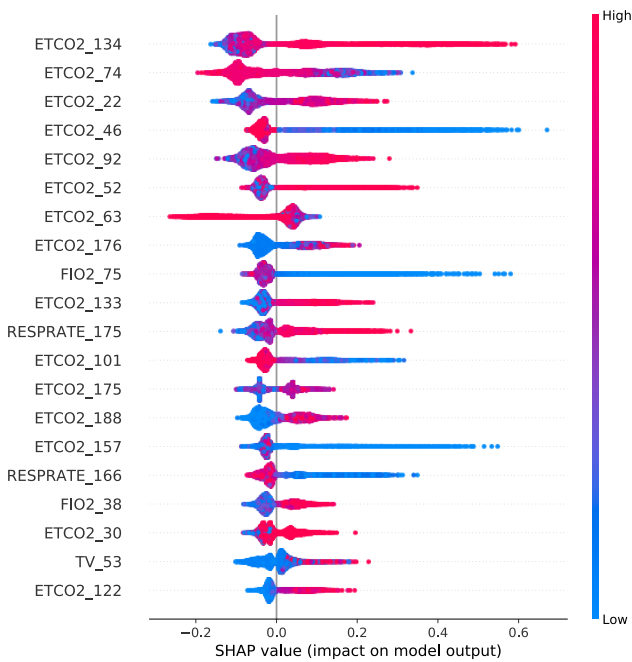
a.) Per-feature attributions for *raw*



b.) Aggregated attributions for *raw*



c.) Per-feature attributions for *next*



d.) Aggregated attributions for *next*

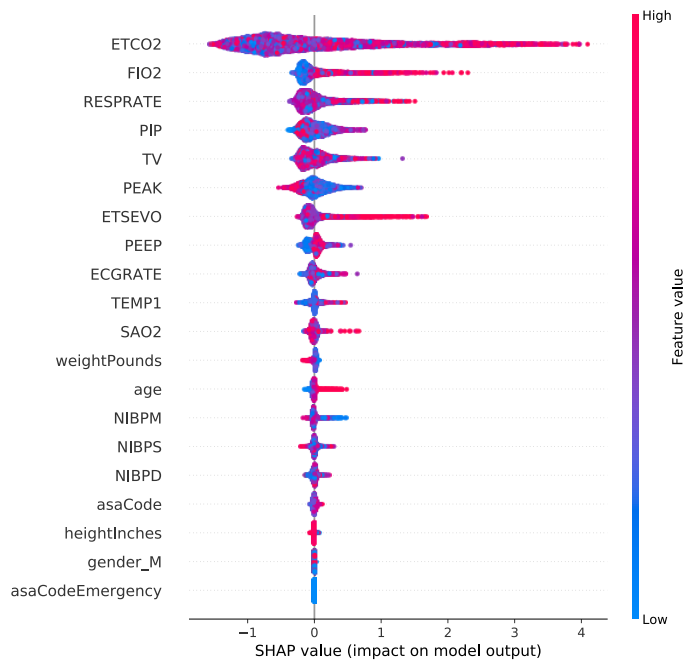
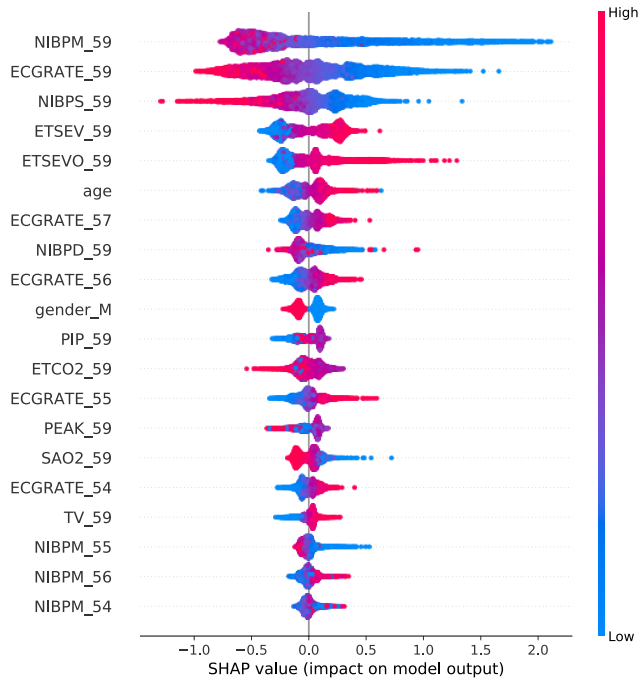
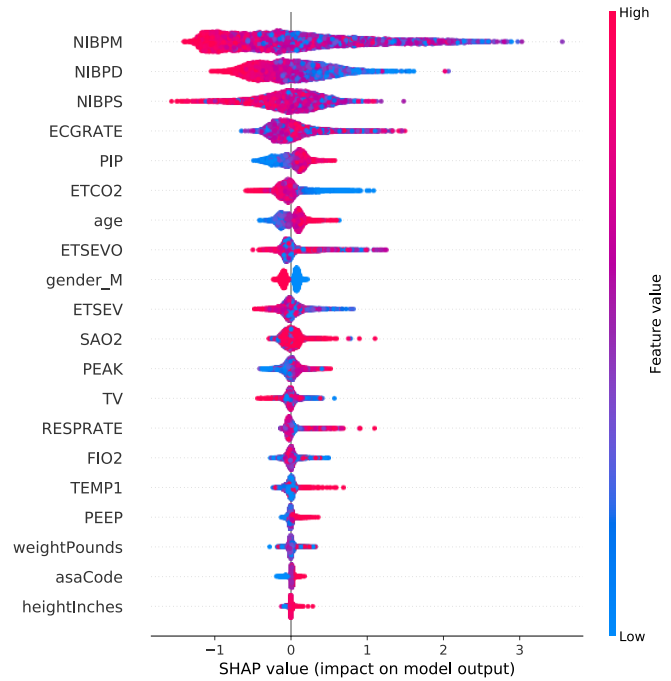


Figure 7: Attributions for *hypocapnia*.

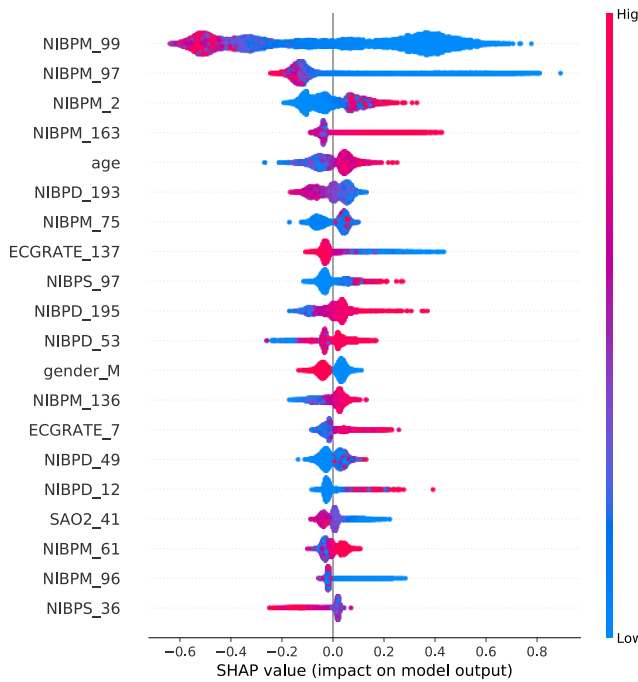
a.) Per-feature attributions for raw



b.) Aggregated attributions for raw



c.) Per-feature attributions for next



d.) Aggregated attributions for next

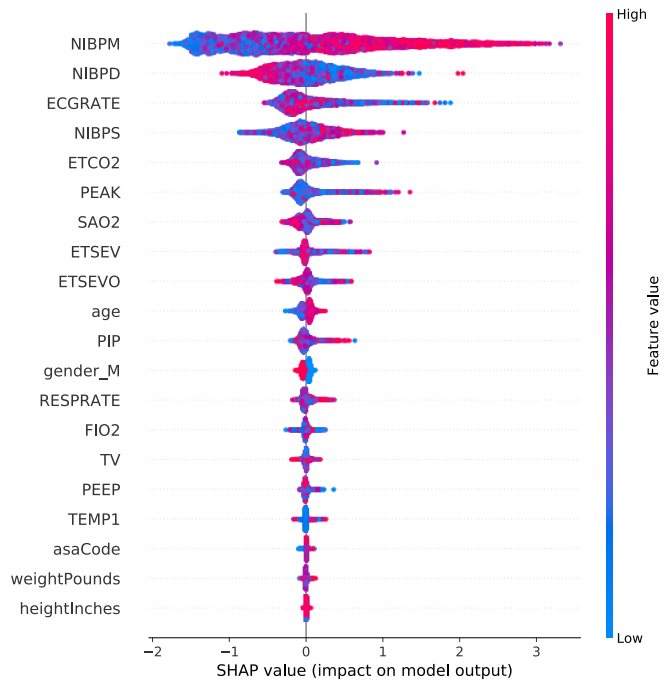
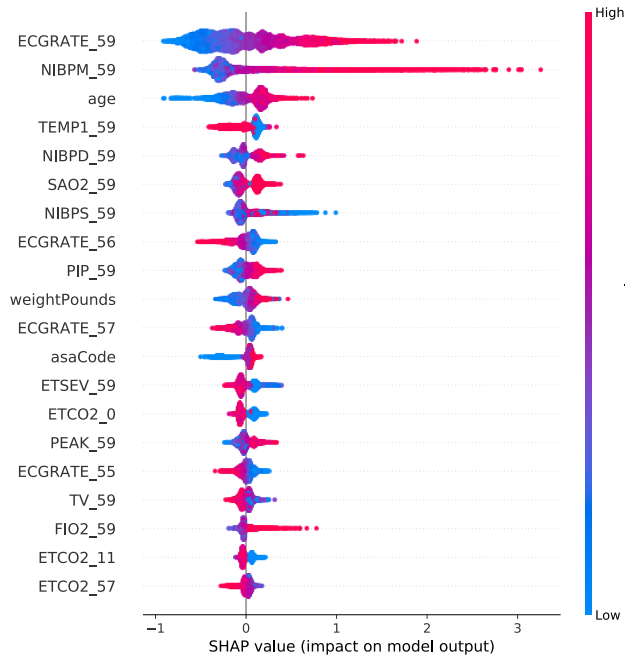
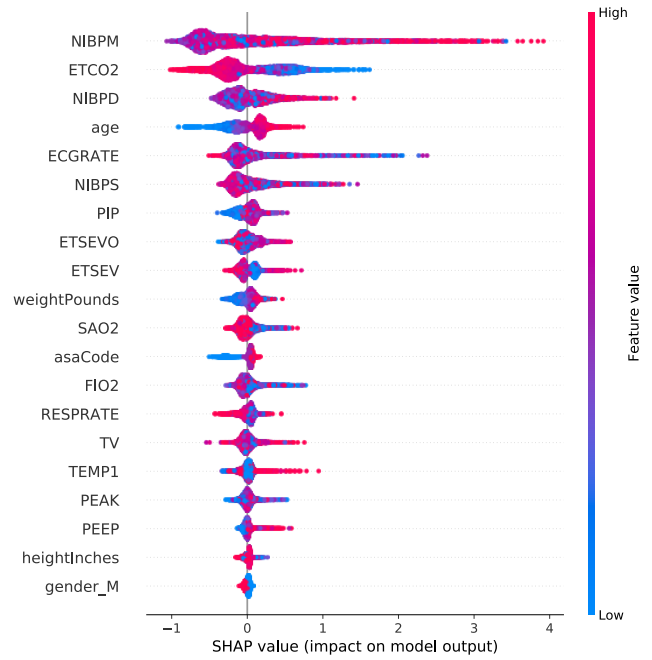


Figure 8: Attributions for hypotension.

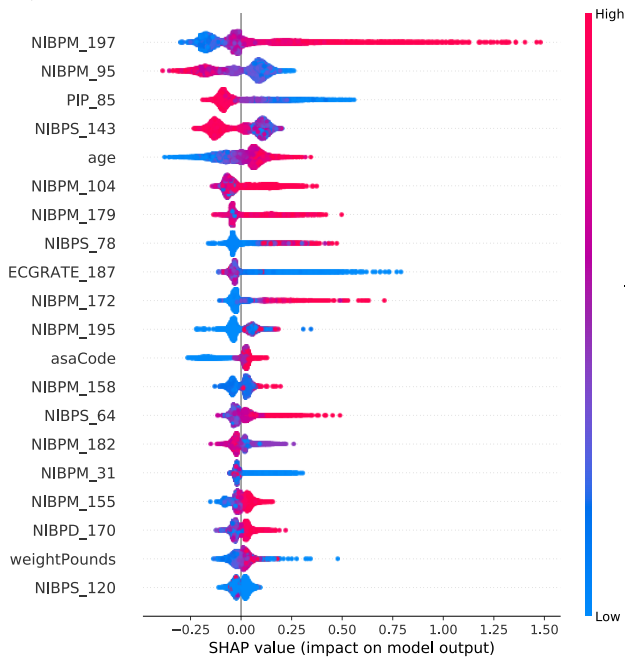
a.) Per-feature attributions for raw



b.) Aggregated attributions for raw



c.) Per-feature attributions for next



d.) Aggregated attributions for next

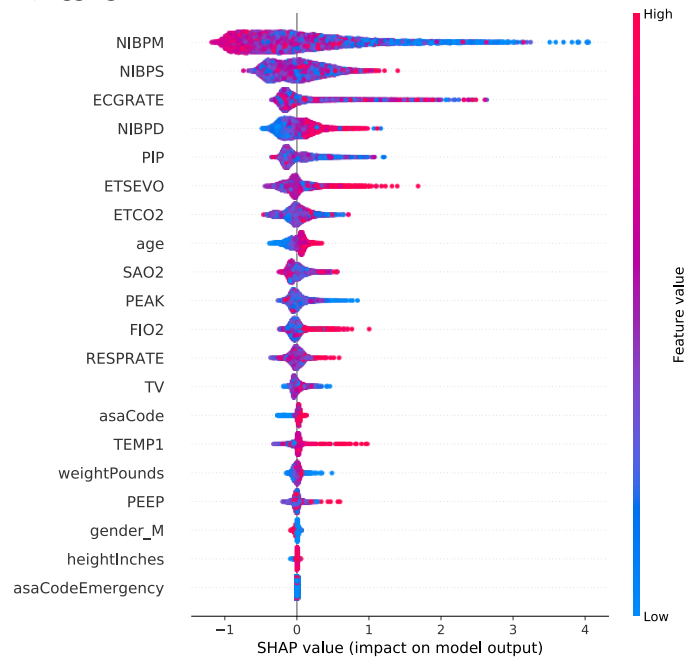
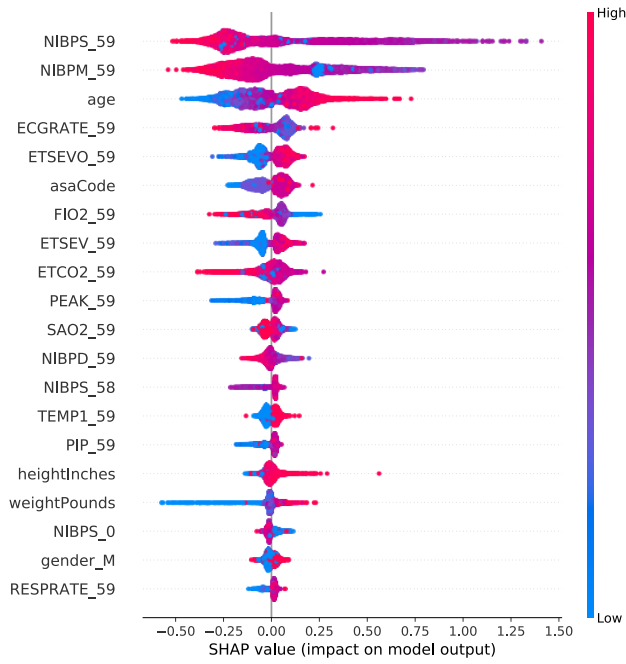
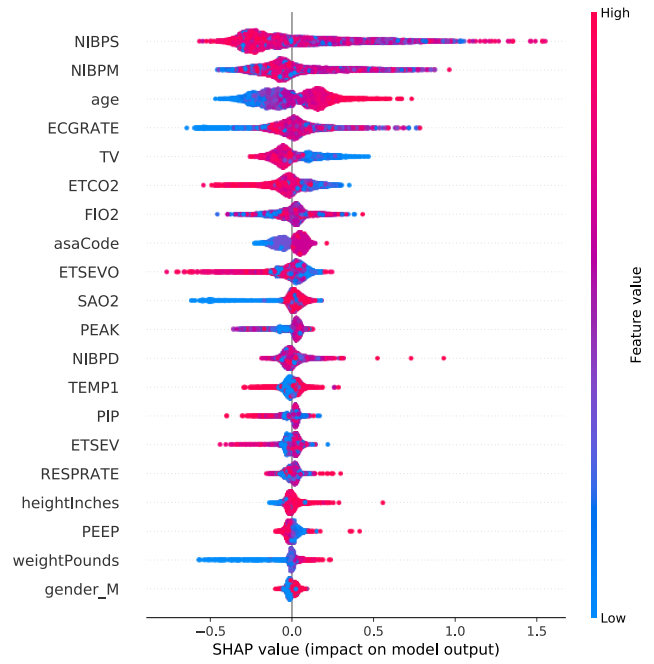


Figure 9: Attributions for hypertension.

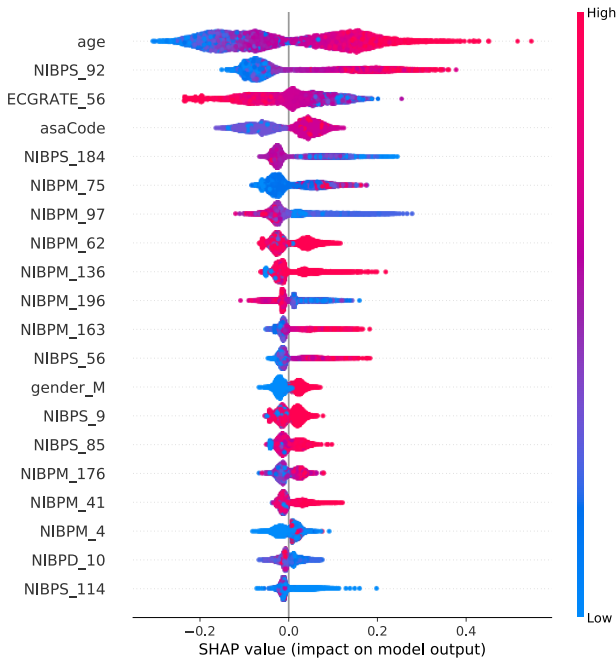
a.) Per-feature attributions for raw



b.) Aggregated attributions for raw



c.) Per-feature attributions for next



d.) Aggregated attributions for next

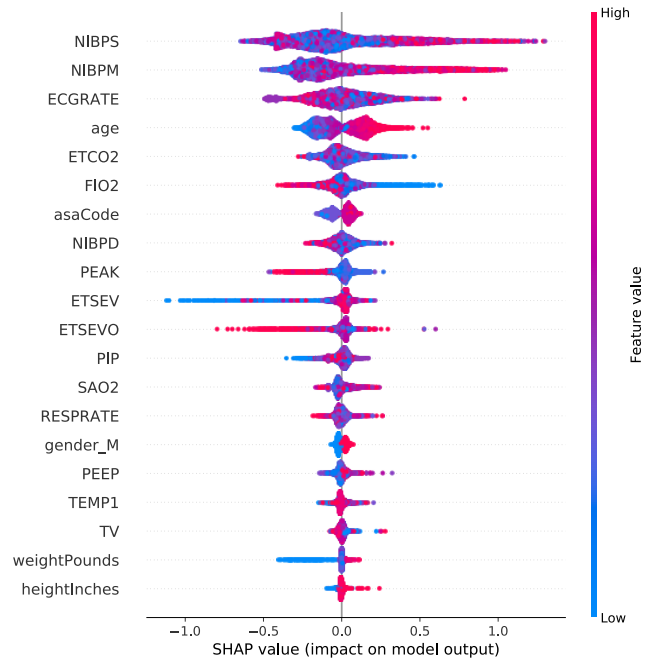


Figure 10: Attributions for phenylephrine.